Supporting information

Regulating interfacial water *via* Ca-doped RuO_x for enhanced acidic oxygen evolution reaction

Gaoliang Fu,* Lina Du, Dengxu Liu, Baocheng Yang and Shouren Zhang*

Henan Provincial Key Laboratory of Nanocomposites and Applications, Institute of Nanostructured Functional Materials, Huanghe Science and Technology College, Zhengzhou, Henan 450006, China.

E-mail: fugl@hhstu.edu.cn, shourenzhang@infm.hhstu.edu.cn

I. Experiment section

1. Catalyst Synthesis

Ca-doped RuO_x catalysts were synthesized by a two-step synthetic route. First, a 0.08 g mL^{-1} ruthenium chloride hydrate ($RuCl_x \cdot xH_2O$, 99%, Energy Chemical) solution was prepared. 1 mL of this solution was pipetted into a clean beaker, with adding 0.0084 g of $CaCl_2$ powders (AR, 96%, Aladdin). Stirring with a glass rod ensured complete $CaCl_2$ dissolution. Subsequently, 1 g urea (AR, 99%, Aladdin) and 0.2 g of tannic acid (USP, Aladdin) were added. Vigorous stirring for 30 min yielded a uniform dispersion, which was then evaporated to dryness in a preheated 180°C blast oven. The dried solid precursor was transferred to a high-purity alumina crucible and calcined in a muffle furnace at 450 °C for 6 h (heating rate: 5°C min^{-1}). The product was soaked in 1 M HCl for 1 h to remove residual inorganic impurities and dried at 60°C in a vacuum oven for 12 h to obtain the final Ca-doped RuO_x catalysts (Ca-RuO_x). The RuO_x was prepared as the same synthesis method but without adding $CaCl_2$ powder.

2. Material Characterizations

X-ray diffraction (XRD, BRUKER, D8 ADVANCE) was performed using the Cu Kα radiation operating at 40 kV and 40 mA. Scanning electron microscopy (SEM, ZEISS, Sigma 300) and transmission electron microscopy (TEM, JEOL JEM-F200) were employed to investigate the morphology, microstructure and microscopic dimension. Raman (HORIBA, LabRAM HR Evolution) were used to obtain the chemical bonding information. The application of EPR (BRUKER, ESR5000) was introduced to detect the oxygen vacancy. X-ray photoelectron spectroscopy (XPS, Thermo Fisher K-Alpha) was also employed to investigate the valence state of Ru in catalyst using monochromatic Al $K\alpha_1$ X-ray ($h\nu$ = 1486.6 eV). *Operando* attenuated total reflection surface-enhanced infrared absorption spectroscopy (ATR-SEIRAS) were recorded on a Nicolet iS50 FT-IR spectrometer (Thermo Scientific) equipped with MCT-Adetector at different applied potentials.

3. Preparation of electrodes

For OER tests using a conventional three-electrode system, 3 mg of catalysts and 30 μL of Nafion solution (5wt%, aldrich) were dispersed in a mixed solution of 0.22

mL deionized water and 0.08 mL isopropyl alcohol. The mixture was ultrasonicated for 30 minutes to form the homogeneous ink. 30 μL of as-prepared ink was dropped onto a superhydrophilic carbon paper (0.4 cm^2), and then dried under infrared lamp. The dried electrode was used as the working electrode with a catalyst loading of 0.682 mg cm^{-2}.

4. Electrochemical Measurements

The electrochemical measurements were performed on a conventional three-electrode system controlled by CHI760E potentiostat. In the test system, an Ag/AgCl (Saturated KCl) electrode, a platinum mesh and O_2-saturated 0.5 M H_2SO_4 solution (pH = 0.2) were used as reference electrode, counter electrode and electrolyte, respectively. Linear sweep voltammetry (LSV) with potential ranging from 1.0 to 1.4 V (vs. Ag/AgCl) was performed at a scan rate of 0.005 V s^{-1} under a constant magnetic stirring. All the potential during LSV measurements were automatically *i*R-corrected for the ohmic resistance of the solution (95%). Tafel plots was derived from LSV curves. The stability test for catalysts was performed using the chronopotentiometry technology at different current densities (10 mA cm^{-2} and 50 mA cm^{-2}). The electrochemical impedance spectroscopy (EIS) measurements were conducted at different specific potentials at a perturbation amplitude of 5 mV with a sweep frequency range of 100 kHz – 0.1 Hz.

For the electrochemical double-layer capacitance (C_{DL}) measurements, CV data with different scan rates (0.01, 0.02, 0.04, 0.06 and 0.08 V s^{-1}) was collected in the non-Faradaic region potential window of 0.2 V centered at open circuit potential. The electrochemically active surface area (ECSA) of the catalyst is calculated from the double-layer capacitance according the following equation: ECSA = $\frac{C_{DL}}{C_S}$, where C_S is the capacitance of an atomically smooth planar surface of the materials per unit area under identical electrolyte conditions. A general specific capacitances of C_S = 0.035 mF cm^{-2} is used in 0.5 M H_2SO_4.[1]

In the electrochemical analysis, all potentials relative to Ag/AgCl electrode were calibrated to reversible hydrogen electrode (RHE) using the following equation: E (vs.

RHE) = E (vs. Ag/AgCl) +0.199 V + 0.0592 × pH.

5. DFT Calculations

All density functional theory (DFT) calculations were carried out using the Vienna *Ab initio* Simulation Package (VASP)[2, 3] within the generalized gradient approximation (GGA) and the Perdew–Burke–Ernzerhof (PBE)[4] functional. The projector augmented wave (PAW) potentials[5, 6] was employed to describe ionic cores, with valence electrons treated using a plane-wave basis set and an energy cutoff of 450 eV. Van der Waals interactions were included via the DFT-D3 correction. Structural optimizations were performed until the forces were below 0.02 eV/Å and the total energy converged to 1×10^{-5} eV. Brillouin zone sampling was conducted using a (3 × 3 × 1) Monkhorst–Pack k-point mesh.

The Gibbs free energy changes (ΔG) for oxygen evolution reaction (OER) steps were evaluated using the computational hydrogen electrode (CHE) model, where the proton–electron pair chemical potential is referenced to half of the H_2 energy at 0 V vs. RHE. The effect of the applied potential (U) was included as: $G(U) = G(0\ V) – neU$. The Gibbs free energy was calculated as:

$$\Delta G = \Delta E + \Delta E_{ZPE} - T\Delta S \quad (1)$$

where ΔE, $\Delta E_{(ZPE)}$, and ΔS represent the DFT energy, zero-point energy correction, and entropy change at 298.15 K, respectively.

II. Supplementary results

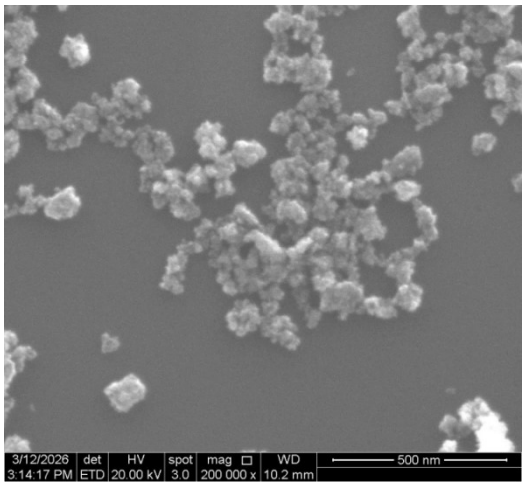

Fig. S1 Scanning electron microsocpy (SEM) image of Ca-RuO_x.

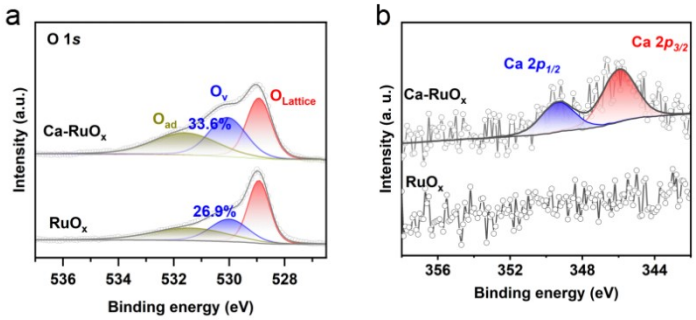

Fig. S2 XPS spectra of Ca-RuO_x and RuO_x. (a) O 1*s*. (b) Ca 2*p*. The high-resolution O 1*s* XPS spectra of Ca-RuO_x and RuO_x (Fig. S2a) are both deconvoluted into three characteristic peaks, corresponding to lattice oxygen (O_L, 529.03 eV), surface adsorbed hydroxyl radicals (O_V, 530.43 eV) and surface adsorbed oxygen (O_{ad}, 532.34 eV), respectively.[7] Among them, surface adsorbed hydroxyl radicals are closely associated to oxygen vacancies.[7] The quantitative analysis shows that the proportion of oxygen vacancies in Ca-RuO_x is 6.7% higher than that in RuO_x.

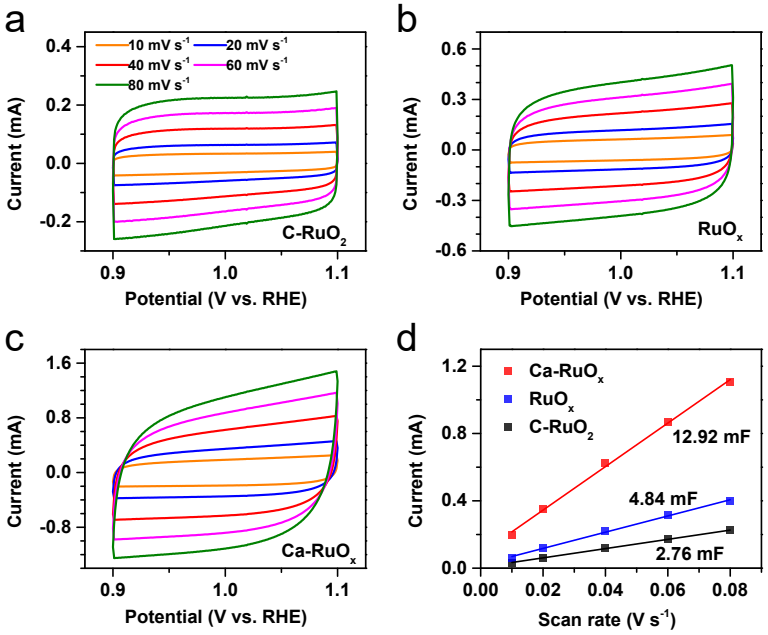

Fig. S3 Double-layer capacitance measurements for determining electrochemically active surface area (ECSA) for Ca-RuO_x and RuO_x from voltammetry in 0.5 M H_2SO_4 solution.[1] Typical cyclic voltammograms in the non-Faradaic region around 1.00 V relative to reversible hydrogen electrode (RHE) at different scan rates (0.01, 0.02, 0.04, 0.06, 0.08 V s^{-1}) for (a) C-RuO_2, (b) RuO_x and (c) Ca-RuO_x. (d) The average of the cathodic and anodic charging currents absolute values measured at 1.0 V (vs. RHE) plotted as a function of scan rate.

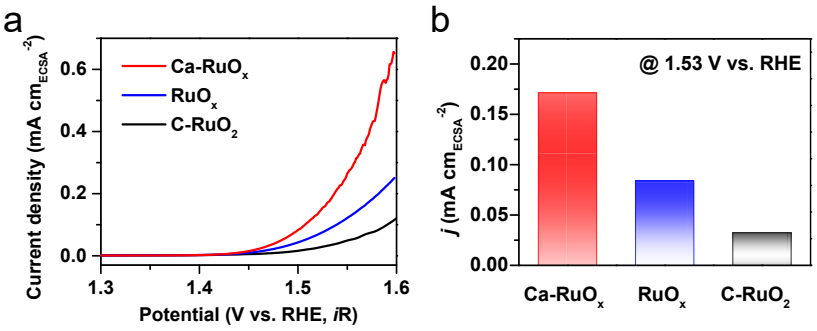

Fig. S4 The OER activities normalized to ECSA surface area. (a) Polarization curves, and (b) the corresponding specific current densities at an anodic potential of 1.53 V vs. RHE.

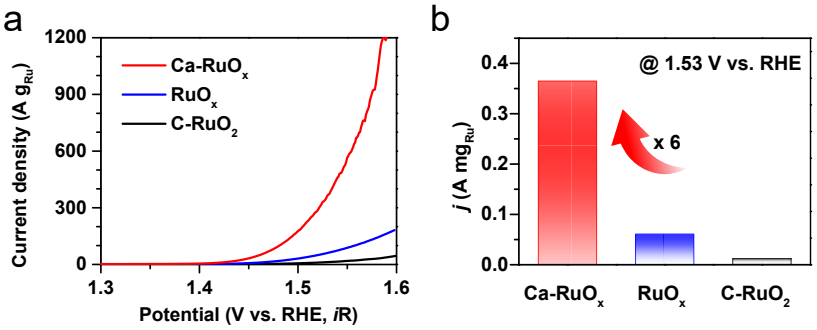

Fig. S5 Mass activities of catalysts. (a) Polarization curves, and (b) the corresponding specific current densities at an anodic potential of 1.53 V vs. RHE.

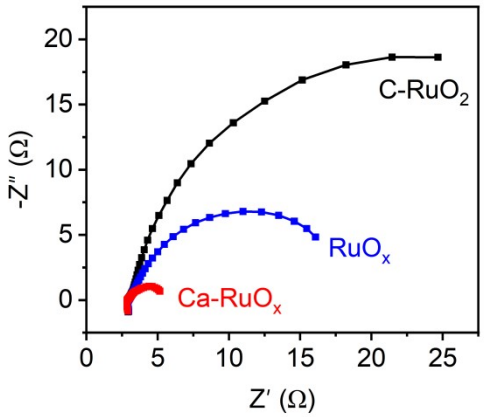

Fig. S6 EIS patterns of Ca-RuOx and RuO_x at 1.5 V (vs. RHE) with a sweep frequency range of 100 kHz to 0.1 Hz. Among them, Ca-RuO_x has a smallest semi-circle, indicating a faster transfer of electrons at the adsorbate-catalyst interfaces for Ca-RuO_x.

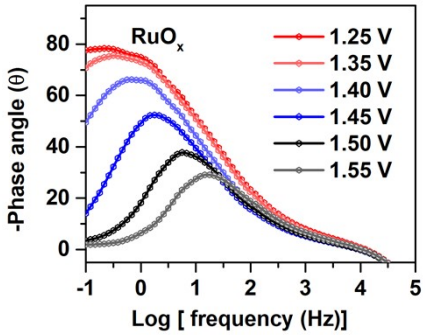

Fig. S7 *Operando* Bode phase plots for RuO_x.

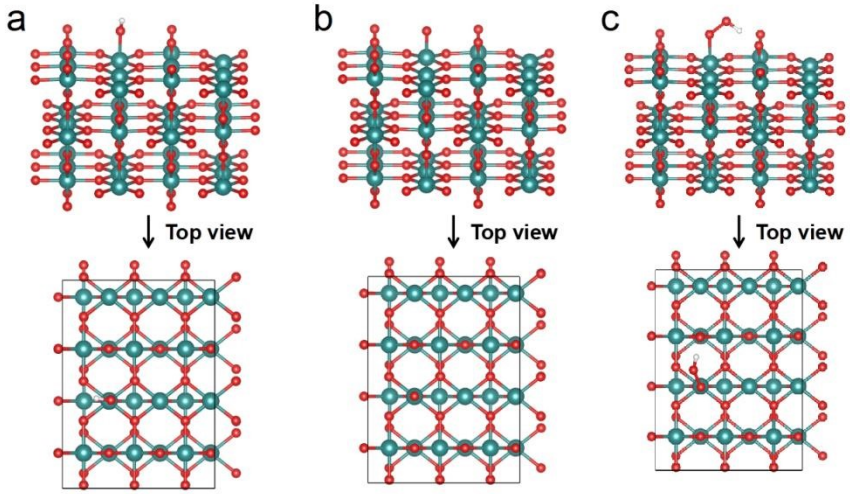

Fig. S8 (a) *OH, (b) *O, (c) *OOH adsorption structures of RuO_2.

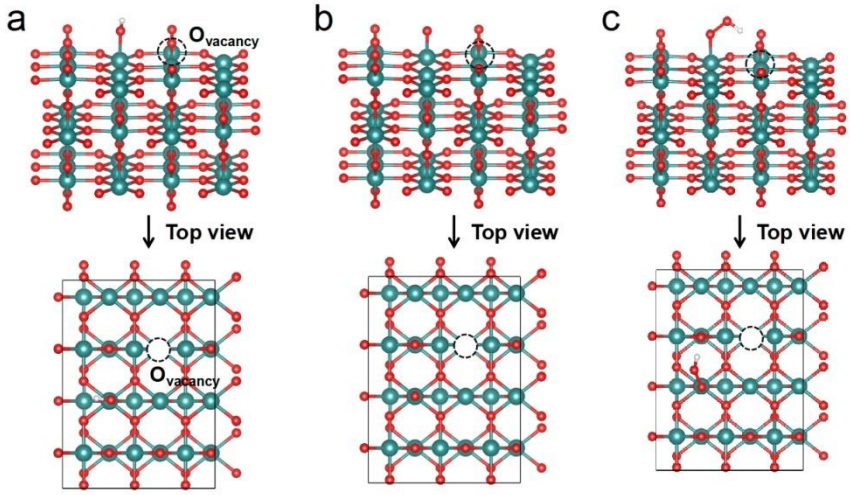

Fig. S9 (a) *OH, (b) *O, (c) *OOH adsorption structures of RuO_x.

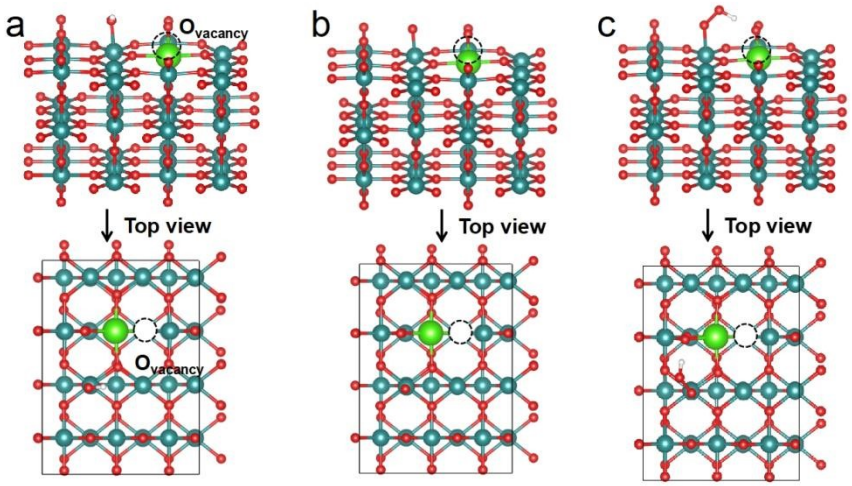

Fig. S10 (a) *OH, (b) *O, (c) *OOH adsorption structures of Ca-RuO_x.

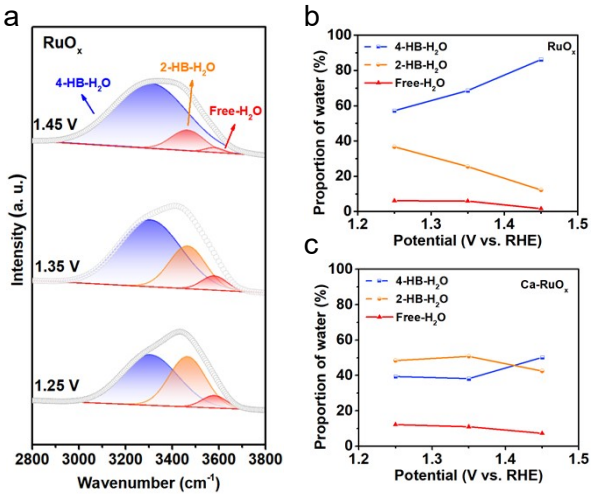

Fig. S11 (a) *Operando* ATR-SEIRAS measurements of RuO_x in the range of 2800 cm^{-1} to 3800 cm^{-1}. The proportions of 4-HB-H_2O, 2-HB-H_2O, and free-H_2O at different potentials for (b) RuO_x and (c) Ca-RuO_x.

Table S1. ICP-AES results of all the samples in this work.

	Ru (wt%)	Ca (wt%)
Ca-RuO_x	63.71	1.17
RuO_x	69.87	~

Table S2. The OER activities of all the samples in this work.

	$\eta_{j=10mA\ cm-2}$ (V)	$\eta_{j=50mA\ cm-2}$ (V)	$j_{ECSA,E=1.53V}$ (mA cm^{-2})	$j_{E=1.53V}$ (A g_{Ru}^{-1})	ECSA (cm^2)
Ca-RuO_x	0.212	0.256	0.171	365	369
RuO_x	0.256	0.331	0.084	61	138
C-RuO_2	0.325	0.418	0.032	12	79

Table S3 Comparison of overpotential (at the current density of 10 mA cm^{-2}) and stability employed in this study with other electrocatalysts.

Sample	Electrolyte	Overpotential	Stability	Ref.
Ca-RuO_x	0.5 M H_2SO_4	212 mV	200 h @10 mA cm^{-2} 200 h @50 mA cm^{-2}	This work
Ga-RuO_2	0.5 M H_2SO_4	218 mV	150 h @10 mA cm^{-2}	Angew. Chem. Int. Ed.[8]
Ba-RuO_2	0.1 M $HClO_4$	229 mV	250 h @10 mA cm^{-2}	J. Energy Chem.[9]
Na/Hf-RuO_2	0.5 M H_2SO_4	238 mV	400 h @10 mA cm^{-2}	Adv. Mater.[10]
$Si_{0.1}RuO_2$	0.1 M $HClO_4$	226 mV	800 h @10 mA cm^{-2}	Nat. Commun.[11]
In-RuO_2	0.5 M H_2SO_4	244 mV	-	Angew. Chem. Int. Ed.[8]
Ni-RuO_2	0.1 M $HClO_4$	214 mV	200 h @10 mA cm^{-2}	Nat. Mater.[12]
$RuCoO_x$	1 M $HClO_4$	200 mV	100 h @10 mA cm^{-2}	J. Am. Chem. Soc.[13]
$La_{0.1}Ru_{0.9}O_2$	0.5 M H_2SO_4	188 mV	63 h @10 mA cm^{-2}	eScience[14]
$Nd_{0.1}RuO_x$	0.5 M H_2SO_4	211 mV	50 h @10 mA cm^{-2}	Adv. Funct. Mater.[15]
Nd-RuO_2	0.1 M $HClO_4$	214 mV	40 h @10 mA cm^{-2}	Nat. Commun.[16]
$Ru_{0.8}Ir_{0.2}O_x$	0.5 M H_2SO_4	189 mV	100 h @10 mA cm^{-2}	Adv. Mater.[17]
Ru_1-Pt_3Cu	0.1 M $HClO_4$	220 mV	28 h @10 mA cm^{-2}	Nat. Catal.[18]
Ru@IrO_x	0.5 M H_2SO_4	282 mV	24 h @1.55 V	Chem[19]
S_H-RuCuO	0.5 M H_2SO_4	231 mV	250 h @10 mA cm^{-2}	Nano Res.[20]

Table S4. Calculated adsorption free energies (ΔG) and the estimated thermodynamic overpotentials (η^{theory}) at U = 1.23 eV for RuO_2, RuO_x and Ca-RuO_x.

Catalyst	$\Delta G_{(* + H2O)}$ (eV)	ΔG_{*OH} (eV)	ΔG_{*O} (eV)	ΔG_{*OOH} (eV)	$\Delta G_{(* + O2)}$ (eV)	(η^{theory}) (eV)
RuO_2	0	-0.536	-0.689	0.175	0	0.864
RuO_x	0	-0.575	-0.721	-0.067	0	0.654
Ca-RuO_x	0	-0.911	-1.045	-0.48	0	0.565

Reference

1. C. C. L. McCrory, S. Jung, J. C. Peters and T. F. Jaramillo, *J. Am. Chem. Soc.*, 2013, **135**, 16977-16987.
2. G. Kresse and J. Furthmüller, *Comput. Mater. Sci*, 1996, **6**, 15-50.
3. G. Kresse and J. Hafner, *Phys. Rev. B*, 1994, **49**, 14251-14269.
4. J. P. Perdew, K. Burke and M. Ernzerhof, *Phys. Rev. Lett.*, 1996, **77**, 3865-3868.
5. P. E. Blöchl, O. Jepsen and O. K. Andersen, *Phys. Rev. B*, 1994, **49**, 16223-16233.
6. G. Kresse and D. Joubert, *Phys. Rev. B*, 1999, **59**, 1758-1775.
7. T. Xu, Q. Liang, F. Liu, Z. Zhao, W. Li, A. Wei, M. Liu, K. Song, B. Yang, T. Dong, X. Zou, W. Zhang and W. Zheng, *Adv. Funct. Mater.*, 2026, **36**, e22894.
8. L. Wu, W. Huang, D. Li, H. Jia, B. Zhao, J. Zhu, H. Zhou and W. Luo, *Angew. Chem. Int. Ed.*, 2025, **64**, e202413334.
9. Y. Yang, J. Guo, L. Xu, C. Li, R. Ning, J. Ma and S. Geng, *J. Energy Chem.*, 2025, **102**, 1-9.
10. Y. a. Zhu, F. Wu, X. Zhang, Y. Lin, L. Zhang, T.-S. Chan, Q. Zhang and L. Chen, *Adv. Mater.*, 2025, **37**, 2500449.
11. X. Ping, Y. Liu, L. Zheng, Y. Song, L. Guo, S. Chen and Z. Wei, *Nat. Commun.*, 2024, **15**, 2501.
12. Z.-Y. Wu, F.-Y. Chen, B. Li, S.-W. Yu, Y. Z. Finfrock, D. M. Meira, Q.-Q. Yan, P. Zhu, M.-X. Chen, T.-W. Song, Z. Yin, H.-W. Liang, S. Zhang, G. Wang and H. Wang, *Nat. Mater.*, 2023, **22**, 100-108.
13. W. Zhu, F. Yao, K. Cheng, M. Zhao, C.-J. Yang, C.-L. Dong, Q. Hong, Q. Jiang, Z. Wang and H. Liang, *J. Am. Chem. Soc.*, 2023, **145**, 17995-18006.
14. C.-H. Li, C.-Z. Yuan, X. Huang, H. Zhao, F. Wu, L. Xin, X. Zhang, S. Ye and Y. Chen, *eScience*, 2025, **5**, 100307.
15. L. Li, G. Zhang, J. Xu, H. He, B. Wang, Z. Yang and S. Yang, *Adv. Funct. Mater.*, 2023, **33**, 2213304.
16. X. Zhang, Y. Zhang, B. O. Protsenko, M. A. Soldatov, J. Zhang, C. Yang, S. Bo, H. Wang, X. Chen, C. Wang, W. Cheng and Q. Liu, *Nat. Commun.*, 2025, **16**, 6921.

17. Y. Yuan, H. Fang, K. Chen, J. Huang, J. Chen, Z. Lu, H. Wang, Z. Zhao, W. Chen and Z. Wen, *Adv. Mater.*, 2025, **37**, 2501607.

18. Y. Yao, S. Hu, W. Chen, Z.-Q. Huang, W. Wei, T. Yao, R. Liu, K. Zang, X. Wang, G. Wu, W. Yuan, T. Yuan, B. Zhu, W. Liu, Z. Li, D. He, Z. Xue, Y. Wang, X. Zheng, J. Dong, C.-R. Chang, Y. Chen, X. Hong, J. Luo, S. Wei, W.-X. Li, P. Strasser, Y. Wu and Y. Li, *Nat. Catal.*, 2019, **2**, 304-313.

19. J. Shan, C. Guo, Y. Zhu, S. Chen, L. Song, M. Jaroniec, Y. Zheng and S.-Z. Qiao, *Chem*, 2019, **5**, 445-459.

20. Q. Yao, Z. Yu, Y.-H. Chu, Y.-H. Lai, T.-S. Chan, Y. Xu, Q. Shao and X. Huang, *Nano Res.*, 2022, **15**, 3964-3970.